JOURNAL OF MATERIALS SCIENCE 23 (1988) 1112–1125

Influence of additions on the solidification behaviour of Ni–B alloys – crystallography of Ni–Ni_3B eutectic

J. AJAO, S. HAMAR-THIBAULT
Institut National Polytechnique de Grenoble, L.T.P.C.M. (C.N.R.S.-UA. 29), Domaine Universitaire, B.P. 75, 38402 St Martin d'Heres, France

The influence of small additions (1 to 2 at.%) of some elements (chromium, copper, silicon, aluminium, iron, titanium, vanadium) on the solidification behaviour and crystallography of Ni(α)–Ni_3B eutectic composition is examined by differential thermal analysis, X-ray and electron diffractions, scanning and transmission electron microscopy. With the exception of Fe-doped eutectic alloys, all the alloys whether doped or undoped exhibit a very large undercooling for the nucleation of Ni_3B. We give an interpretation of the controversial hypothesis of this undercooling. We propose a crystallographic orientation relationship between the cubic phase Ni(α) and the orthorhombic phase Ni_3B in the lamellar eutectic Ni–Ni_3B. We also examine a complex transformation which occurs in Ni_3B during slow cooling.

1. Introduction

Hardfacing is an important feature for all problems of wear and corrosion. For many uses, wear and corrosion are connected and the alloys must show good wear and corrosion resistant properties [1–3]. Hardfacing alloys are characterized by a dispersion of hard phases of several kinds (carbides, borides and silicides) in an fcc matrix. These hard phases are related to the base metals (nickel, cobalt, iron) metallic (chromium, tungsten) and non-metallic (boron, silicon, carbon) additions [1, 4].

The autofluxing properties of nickel hardfacing alloys make these alloys interesting for some industries (chemical and glass industries [1–3]). In spite of numerous studies, only few works report microstructural and microscopic features [1, 4]. The wear resistance is directly connected to the relations between the matrix and the hard phases: nature (boride, silicide, carbide), distribution, form and dimensions, orientation relationship between the phases. Among the eutectics present in these alloys, the Ni(α)–Ni_3B eutectic is very common.

Kolomytsev [5] confirmed the existence of the boride Ni_3B earlier detected through X-ray diffraction studies by Anderson and Kiessling [6]. This boride has been synthetically prepared and electrochemically separated from binary alloys containing more than 0.03 at.% B by this author. Rundqvist [7] obtained X-ray diffraction data and showed that the lattice of this boride is isomorphous with the cementite lattice (type Fe_3C) and belongs to the space group Pbnm.

In their studies of the equilibrium phase diagram of Ni–B, Portnoi *et al.* [8] observed the eutectic composition Ni(α)–Ni_3B to be at 19 at.% B and the eutectic temperature of 1110° C. On the other hand, Schöbel and Stadelmaier [9] reported the eutectic temperature to be 1093° C for the composition of 17 at.% B. The phase diagram Ni–B was calculated by Jansson and Agren [10]. Fig. 1 shows the equilibrium diagram proposed in the region of the Ni–Ni_3B eutectic.

In fact, there are some controversial points in the equilibrium diagram of the binary system Ni–B among the different authors. The main difference is the possibility of a metastable eutectic Ni(α)–Ni_2B at 986° C proposed by Schöbel and Stadelmaier [9] and later confirmed by Knotek and Lugscheider [1]. This phenomenon was interpreted by a simple supercooling of these alloys in the works of Portnoi *et al.* [8] and Sobolev and Fedorov [11]. This stimulates us to examine more deeply the solidification behaviour of Ni–B alloys in the composition range 0 to 30 at.% B and the influence of additions such as iron, aluminium, copper, chromium, silicon, titanium and vanadium. Table I gives the crystallographic data of the phases mentioned in this work.

Some authors have studied the crystallography of unidirectionally solidified Ni(α) and Ni_3B eutectic and obtained some orientation relationship between the two phases [12]. We have also studied the crystallography of this eutectic and paid more attention to the influence of additions.

2. Experimental procedure

A series of alloys from 2 to 30 at.% B were prepared. These alloys were prepared from pure Ni and NiB containing 15 wt % B. To the eutectic composition were added pure elements (0.5 to 2 at.%). Accurately weighed components of each alloy were arc-melted in an argon atmosphere using a non-consumable tungsten electrode. This operation was repeated two or three times to ensure the homogeneization of these samples.

The melting behaviour and the phase formation were determined by differential thermal analysis

0022–2461/88 $03.00 + .12

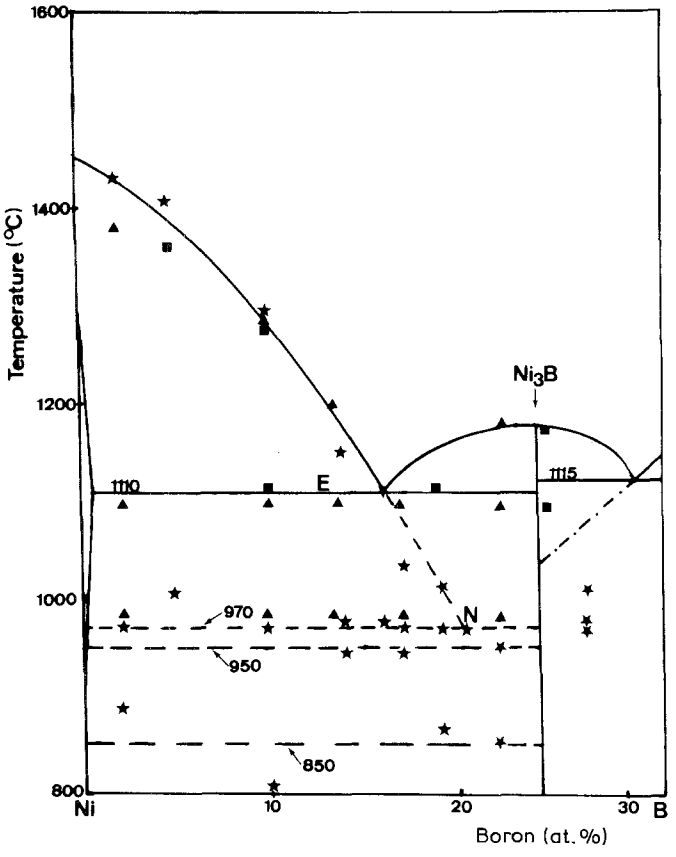

Figure 1 Ni–B equilibrium diagram in the nickel-rich region. (■) Portnoi *et al.* [8], (-·-·-·-, ▲) Schobel and Stadelmaier [9], (★) present work.

(DTA) in a semi-quantitative automatic apparatus developed in our laboratory [13]. This apparatus allows the automatic control of thermal programs and automatic analysis of the results. The heating and cooling rate is 5° C min^{-1}. We also examined samples quenched from the liquidus.

The microstructure of the samples was examined using optical microscopy and scanning electron microscopy (SEM-JSM35) equipped with energy dispersive X-ray analysis system (EDEX-TRACOR). The samples for SEM observations were slightly etched with an etchant consisting of 5 g $FeCl_3$ + 10 ml HCl dissolved in 50 ml H_2O.

The nature of the phases present in these samples was examined by X-ray diffraction. More accurate characterizations were obtained by transmission electron microscopy (TEM) and electron diffraction performed on thin foils in a JEM-200CX. EDX analyses were obtained on STEM-VG-HB5 with a resolution of 1.5 nm at the sample level. Thin foils were obtained by electropolish in an electrolyte containing 57% H_2SO_4 in H_2O at room temperature under 10 V. Some thin foils were prepared by ion bombardment.

TABLE I Crystallographic structure of some compounds

Compound	Space group		Lattice parameter (nm)			Reference
			a	*b*	*c*	
Ni	Fm3m	A1	0.352			[21]
Ni_3B	Pbnm	Do_{11}	0.4389	0.5211	0.6619	[7]
Ni_2B	14/mcm	C_{16}	0.499		0.424	[26]
$Ni_{21}Ti_3B_6$	Fm3m	$D8_4$	1.057			[15]
$\beta 1Ni_3Si$	Fm3m		0.351			[25]

3. Experimental results

3.1. Solidification behaviour of Ni–B alloys (B < 30 at.%).

3.1.1. Quenched from liquidus Ni–B alloys

Rapidly cooled alloys show a large domain of composition from 15.3 to 16.2 at.% B which exhibit a lamellar eutectic microstructure. The Ni–16.2 at.% B alloy shows the most regular eutectic (Fig. 2b), and the lamellar spacing is about 0.5 μm. In this case, the cooling rate could be estimated at 10° C sec^{-1} [13] between the liquidus and the solidus temperatures. As shown in Fig. 3, observations by TEM show that the eutectic formed by these cooling conditions is well defined with the two phases Ni(α) and Ni_3B as shown on the diffraction pattern (Fig. 3c).

In 10 at.% B alloy, the primary phase Ni(α) (Fig. 2a) is surrounded by a halo of Ni_3B formed from rejected boron atoms from nickel, and a well-defined binary eutectic Ni(α)–Ni_3B. For higher boron content (16,9 at.%) (Fig. 2c), Ni_3B is the primary phase as expected on the binary diagram (Fig. 1).

The heating of these quenched hypo and eutectic alloys analysed by DTA presented at least one peak occurring at a fixed temperature (between 1100 and 1110° C). This temperature is representative of the melting of the binary eutectic Ni(α)–Ni_3B.

3.1.2. Slowly cooled alloys

The interpretation of the microstructure and the melting behaviour of rapidly cooled samples is easy. On the other hand, in the case of slow cooling (5° C min^{-1}), the transitions observed during cooling are very difficult to correlate with microstructure. All the alloys with B < 30 at.%, show very large undercooling and the temperatures of the transitions

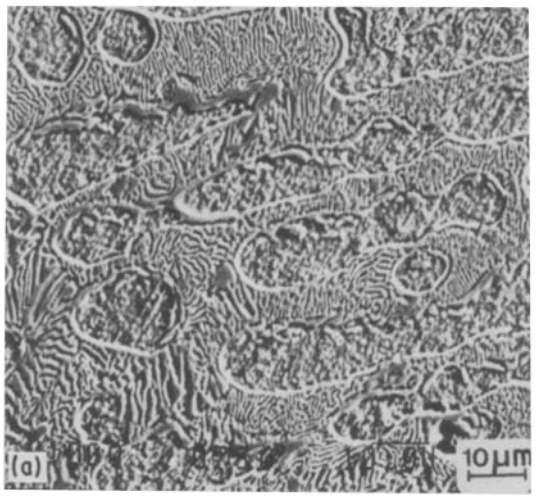

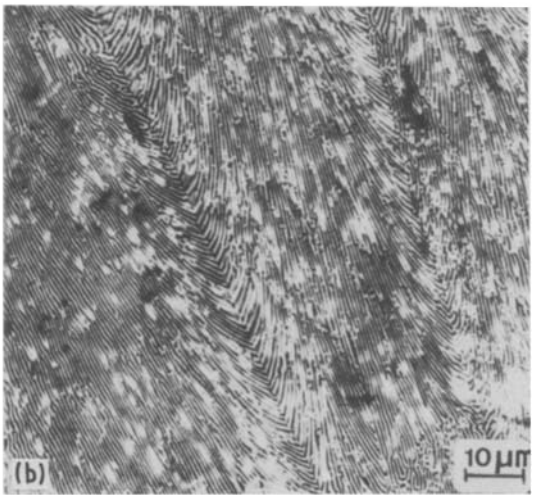

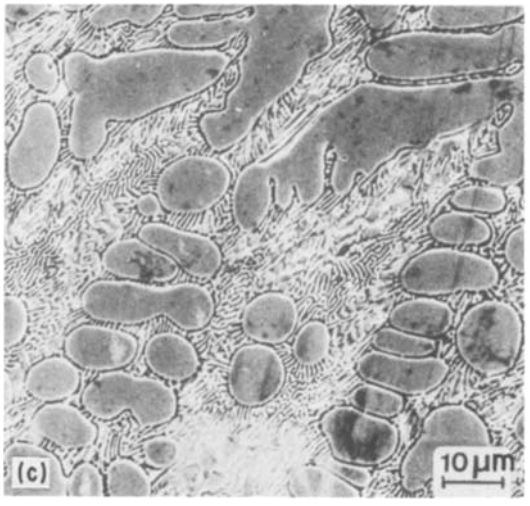

Figure 2 Microstructures of some Ni–B alloys quenched from liquidus. (a) 10 at.% B, (b) 16.2 at.% B, (c) 16.9 at.% B.

(Table II) obtained during slow cooling are completely different from those expected on the binary diagram Ni–B or from the heating results (Fig. 1).

For alloys with a boron content lower than 30 at.%, we observe two or three transitions. The first transition at the highest temperature is due to the solidification of the primary phase Ni(α) or Ni_3B according to the composition. The second transition occurred at a temperature which is lower than expected on the binary diagram (Fig. 1). For the Ni–22 at.% B, the undercooling is maximum (ΔT = 240° C). Moreover, we observe a third transition within a low range of temperature (800 to 850° C) in the hypoeutectic alloys. The quantity of heat released associated with this transition is important (10% of the heat released associated with the second transition).

Even for a boron level higher than 20 at.%, the microstructure of the slow cooled samples always shows Ni(α) dendrites to a certain extent. In the Ni–15.3 at.% B alloy, quantitative determination of the heat released during the Ni(α) dendrite solidification gives the amount of the primary phase to be 5%. The Ni–19.2 at.% B alloy shows some Ni(α) dendrites (1%) as shown in Fig. 4. Because of this small amount of Ni(α), a small exothermic peak is observed at 1018° C (Table II). Alloys with a higher boron content (30 at.%) show microstructures with intermetallic borides as primary phases.

For all the slowly cooled alloys with B < 30 at.%, the interdendritic phase shows a particular microstructure as reported on Fig. 4. This figure presents the morphology of the interdentritic phase for alloys with different compositions (5, 10 and 19.2 at.% B). Accurate observations of this interdendritic phase show that the second phase is not homogeneous and has certainly undergone a solid-state transformation during cooling. This solid-state transformation is associated with the transition observed at the lowest temperature (between 950 and 800° C) and will be discussed later (Section 3.4).

TABLE II Transition temperatures observed in DTA experiments in the Ni–B system

	B (at.%)	Transition temperatures (DTA)					
		Cooling			Heating		
1	2	1432	970	880	1376	1114	
2	5	1416	1004	860		1126	
3	10	1295	970	808	1295	1114	
4	14	1156	980	942	1161	1110	
5	15.3	1104	974		1122	1108	
6	16.2	1110	980		1126	1118	
7	16.9	1032	971	944	1152	1118	
8	19.2	1018	970	862	1140	1110	
9	21		970		1167	1114	
10	22		952	853	1125	1095	
11	25	1085	1066	1006	1156	1118	1020
12	26.8	1004	987	974	1174	1102	
13	30	1082	1030	991	1115		1009

3.2. Influence of additions on the solidification behaviour

3.2.1. Quenched ternary alloys from liquidus

Generally with small additions (0.5 to 1%) to the eutectic (Ni–16.2 at.% B) composition, we observed a small shift of this eutectic composition. The formation of a small amount of primary phases depends on the nature of the element. This primary phase is Ni(α) for all the added elements (Figs 5a, b) with the exception of V-doped eutectic alloy where the primary dendrites are Ni_3B (Fig. 5c).

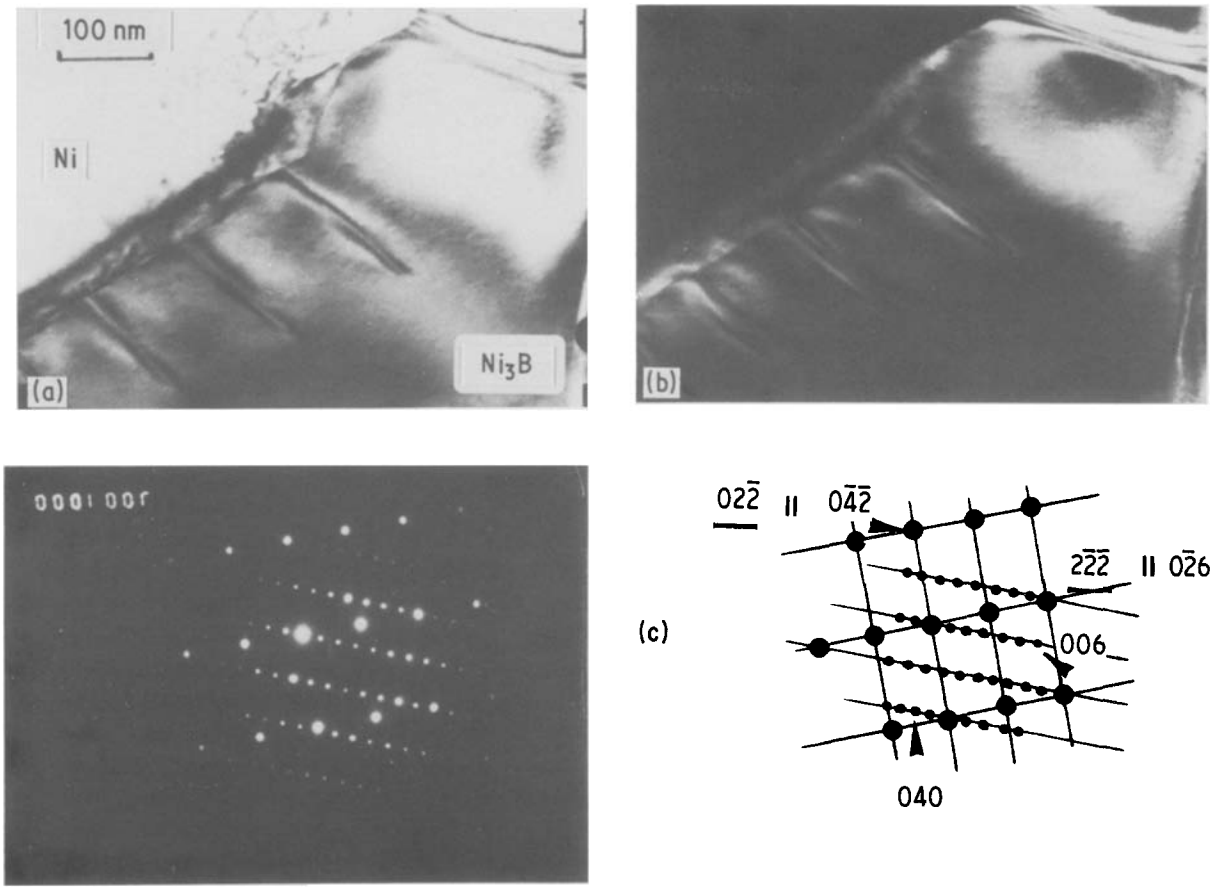

Figure 3 Transmission electron micrograph of Ni–16.2 at.% B. (a) Bright field and (b) dark field. (c) Superposed diffraction pattern and key diagram: (●) Ni, (•) Ni_3B.

Different types of solidification behaviour are observed. First, chromium, aluminium, iron, silicon and copper additions (1 at.%) do not modify significantly the microstructure of the rapidly cooled eutectic (Fig. 5a). As in undoped eutectic alloys, the primary dendrites Ni(α) are surrounded by a small halo of Ni_3B (Fig. 2a). The lamellar spacing in the Ni–Ni_3B eutectic is almost the same (from 0.3 to 0.8 μm) as in the binary eutectic without additions (Fig. 2b).

In the case of titanium and vanadium additions, the microstructures of the rapidly cooled alloys are complex compared to alloys with other additions. The microstructure of the rapidly cooled titanium samples shows Ni(α) primary dendrites and a large amount of binary eutectic Ni–Ni_3B (Fig. 5b). A quantitative analysis performed on this alloy shows that about 0.16 at.% Ti is present in the dendrites. All titanium is rejected in the interdendritic groove where a small amount of a second eutectic with a very fine structure is observed at the end of the solidification. Deeper observations with TEM of Ni(α) dendrites in the Ni–16.2 at.% B–1 at.% Ti show that precipitation occurred in the nickel dendrites. Fig. 6 shows a transmission electron micrograph of this precipitated phase in coherency with the matrix and the key diagram of the diffraction pattern. This phase is indexed as the ternary phase $Ni_{20}Ti_3B_6$ (τ-phase) with an f c c structure of the type $Cr_{23}C_6$ with $a = 3a_0 = 1.057$ nm [14], where a_0 is the lattice parameter of the Ni(α) matrix.

During heating, all doped quenched binary eutectic alloys show a large endothermic peak between 1090 and 1100° C corresponding to the melting of the binary eutectic Ni–Ni_3B. This temperature is close to those measured in the undoped eutectic alloy.

3.2.2. Slowly cooled samples

In the slowly cooled samples, three typical microstructures are observed. With the exception of Fe-doped eutectic alloy, all the slowly cooled alloys show Ni(α) as primary phases. Slowly cooled Cr- or Al-doped eutectic (Fig. 7b) alloys show a rough microstructure with the two phases Ni and Ni_3B. On the other hand, Cu-, Ti- and V-doped eutectic alloys (Fig. 7c, d) show an interdendritic phase which is very similar to those observed in the binary alloys with the transformed structure (Fig. 4c). This structure is observed in Cu- or V-doped eutectic alloys as interdendritic phase or in Ti-doped eutectic alloys where it participates in a binary eutectic with other phases (the τ-phase as in Fig. 7c). The microstructure of the slowly cooled Fe-doped eutectic alloy is shown in Fig. 7a. Apart from some primary phase (Ni_3B), the rest of the structure is a lamellar, well-orientated binary eutectic between Ni(α) and Ni_3B. The lamellar spacing is about 4.5 μm.

During slow cooling, all samples exhibit two or three exothermic peaks in DTA (Table III). The solidification behaviour with chromium additions is similar to that of a hypoeutectic alloy without any additions. The first transition occurs at 1095° C, about 20° C below the corresponding one in the binary system. In the case of other additions (aluminium,

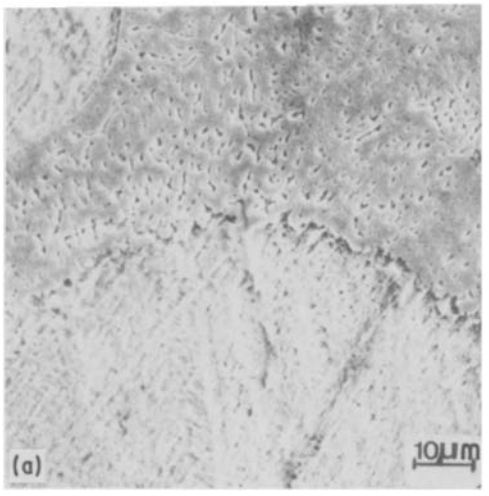

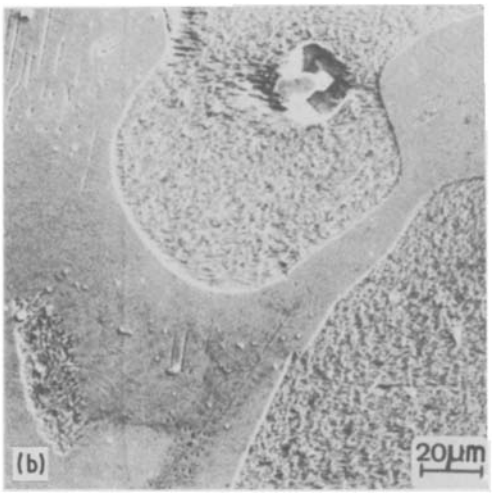

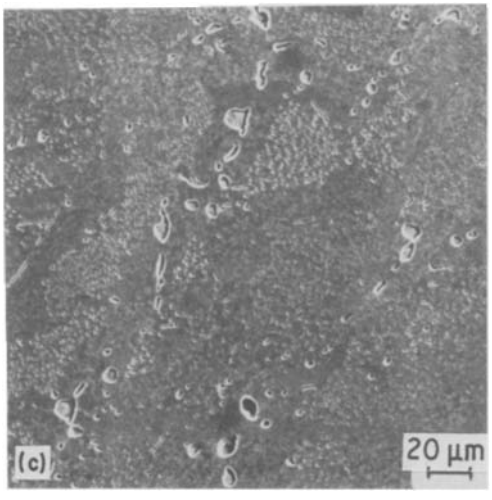

Figure 4 Microstructures of some slowly cooled Ni–B alloys (5° C min^{-1}). (a) 5 at.% B, (b) 10 at.% B, (c) 19.2 at.% B.

copper, titanium, vanadium) the transition occurring between 1140 and 1150° C, and corresponding to the formation of small quantities of Ni(α) dendrites is observed at a higher temperature than in the binary eutectic (T = 1118° C). However, the slowly cooled Fe-doped eutectic alloy shows its first transition at 1104° C and corresponds to the formation of the primary dendrites of Ni_3B, while that of 1096° C is due to the crystallization of the lamellar eutectic Ni(α)–Ni_3B. As shown in Fig. 7a, the binary eutectic nucleates on the primary Ni_3B phase.

With the exception of Fe- and Ti-doped eutectic alloys, the temperature of the second transition is observed between 980 and 950° C in the same range as those of undoped eutectic alloys. From the microstructure of the samples, this transition is related to the formation of the rough structure between Ni_3B and Ni(α) observed in Cr- or Al-doped eutectic alloys (Fig. 7b). In the case of Ti-doped eutectic alloy (Table III), the DTA experiments show four transitions. Two transitions are related to the solidification of the binary eutectic (Ni-τ) and the ternary eutectic (Ni_3B–Ni-τ). As in binary system, a transition at low temperature (900 to 800° C) is observed in Cu-, V- and Ti-doped eutectic alloys, and is related to the microstructure reported previously as the transformed structure of Ni_3B.

Addition of two types of elements 0.5 at.% Fe + 0.5 at.% (Cr, Ti or V) shows that the structure of the rapidly cooled alloys is similar to that observed in alloys with addition of chromium, titanium or vanadium with no marked changes. The microstructure of the slowly cooled Fe + Cr-doped eutectic alloy is identical to that of the slowly cooled Cr-doped eutectic alloy while that of Fe + (Ti, V)-doped eutectic alloys is similar to that of Ti- and V-doped eutectic alloys, respectively. As observed with single additions, these alloys show only one transition during heating in DTA experiments. During slow cooling, the solidification behaviour of alloys with these double additions is comparable to those observed with a simple addition.

TABLE III Effect of addition on the transition temperatures of the Ni–16.2 at.% B–M% alloys. Nature of the primary phase

Nature of addition, M (at.%)	Transition temperatures (DTA)					Primary phase
	Cooling				Heating	
	1110	980			1118	Ni
Fe 1%	1104	1096			1090	Ni_3B
Cr 1%	1096	976			1096	Ni
Al 1%	1147	980			1080	Ni
Cu 1%	1142	950		924	1096	Ni
Si 1%	1126	978		942	1100	Ni
Ti 1%	1151	1004	995	905	1095	Ni
V 1%	1138	954		875	1093	Ni
Fe + Cr 0.5%	1140	971			1110	Ni
Fe + Ti 0.5%	1136	998		844	1101	Ni
Fe + V 0.5%	1144	988		876	1110	Ni

3.3. Crystallography of the Ni(α)–Ni_3B lamellar eutectic

The transmission electron micrograph in Fig. 3a shows that the two phases of the quenched eutectic are: (i) the Ni(α) solid solution, (ii) a second phase which is well indexed with the Ni_3B structure [7].

The relative orientation relationship between the Ni_3B and Ni(α) could be deduced from the combined Ni/Ni_3B electron diffraction patterns. The best fitting is represented by the typical diffraction pattern shown in Fig. 3c, which is indexed in the accompanying diagram. The orientation relationship may be described as:

$$\langle 1\,0\,0\rangle Ni_3B \parallel \langle 2\,1\,1\rangle Ni$$

$$(0\,1\,\bar{3})Ni_3B \parallel (\bar{1}\,1\,1)Ni$$

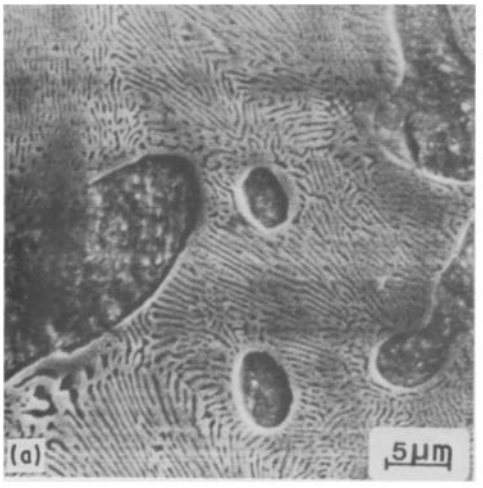

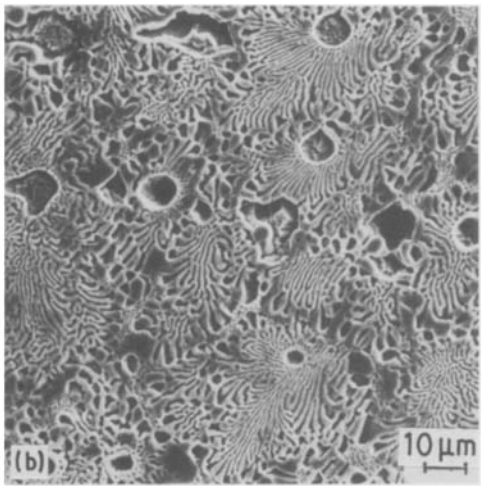

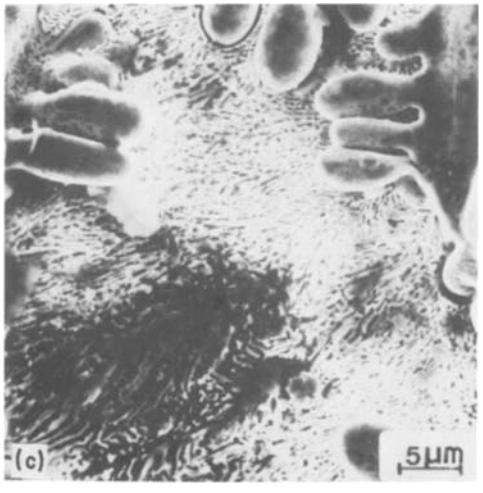

Figure 5 Microstructures of some doped eutectic alloys (1 at.%) quenched from liquidus. (a) Cr, (b) Ti, (c) V.

and

$$(0\,4\,2)Ni_3B \parallel (0\,\bar{2}\,2)Ni$$

On the basis of this orientation relationship, the stereogram between the two phases is constructed (Fig. 8) around $(1\,0\,0)Ni_3B$ and $(2\,1\,1)$Ni planes. This superimposed stereogram shows that the $(1\,0\,0)$, $(0\,1\,0)$ and $(0\,0\,1)$ planes of Ni_3B are, respectively, parallel to high reticular planes of nickel, and close to the $(2\,1\,2)$, $(1\,3\,1)$ and $(1\,1\,3)$ Ni_3B planes. The interface plane is $(1\,1\,4)Ni_3B \parallel (1\,3\,0)$Ni.

The eutectic structure was held at different temperatures (750, 900° C) during heating in DTA experiments and quenched in water upon removal from the furnace (Fig. 9). The coarsening of the structure seems to proceed with different steps. First, the nickel lamellae collapse at the fault level. Then the faults migrate, and the nickel lamellae disappear during coarsening. At the same time, the interface between Ni and Ni_3B changes as seen in Fig. 9c, indicating that the plane of the interface of the rapidly cooled eutectic is metastable. This coarsening process occurred in localized areas surrounded by regions where the lamellar structure is unchanged as mentioned by different authors during coarsening of lamellar eutectics [15].

Even in the presence of additional elements such as titanium or vanadium (Fig. 10), the orientation relationship between the two phases Ni and Ni_3B rapidly cooled are almost the same as observed in the rapidly cooled undoped eutectic alloy. As previously mentioned, the slowly cooled Fe-doped eutectic sample shows a lamellar structure (Fig. 7a). From superimposed diffraction patterns obtained on this eutectic, we observed the following orientation relationships between the two phases:

$$(1\,1\,1)Ni_3B \parallel (3\,1\,1)Ni$$

and

$$\langle 1\,0\,\bar{1}\rangle Ni_3B \parallel \langle 0\,1\,\bar{3}\rangle Ni$$

This relation is not directly related to our previous results in the rapidly cooled samples.

3.4. Solid state transformation in Ni_3B during slow cooling

The microstructure of the transformed interdendritic phase in the slowly cooled Ni–10 at.% B and Ni–19.2 at.% B alloys (Fig. 4b, c) has been investigated by SEM and TEM. The structure is very complicated. From SEM images, Ni(α) dendrites are observed surrounded by large islands of transformed phase. In this phase, deeper observations with TEM show a very complex structure depending on the location. Fig. 11 presents different features of this phase in the Ni–19.2 at.% B alloy. We observed a sequence from the external to the internal part of the phase: needles, eutectoid-like structure, Ni(α) elongated precipitates and scattered spherical Ni(α) precipitates. All the diffraction patterns are well indexed with the two phases Ni and Ni_3B. From the crystallographic point of view, the directions of the needles, of the lamellar structure and of the precipitates are parallel as shown in the schematic drawing (Fig. 11d).

In the needle region (Fig. 12a), the electron diffraction patterns show only the superposition of two orientations of Ni_3B. Nickel is never detected in this region. The needles are made up of two well-oriented Ni_3B lamellae. The orientation relationship (Fig. 12b) between the two kinds of needle is very simple:

$$(1\,0\,0)1 \parallel (1\,0\,0)2$$

$$(0\,1\,0)1 \parallel (0\,1\,1)2$$

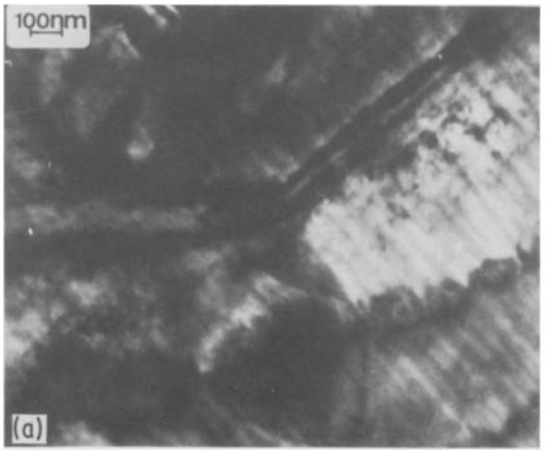

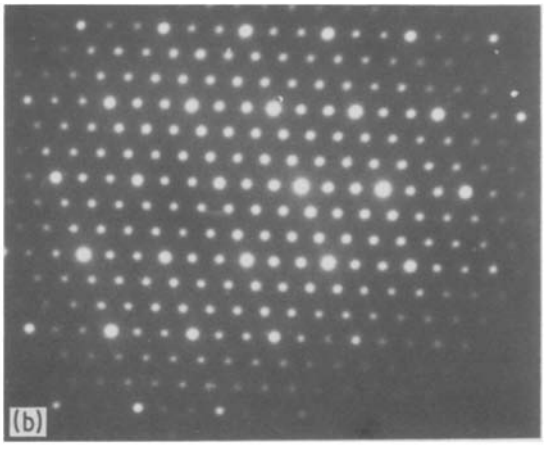

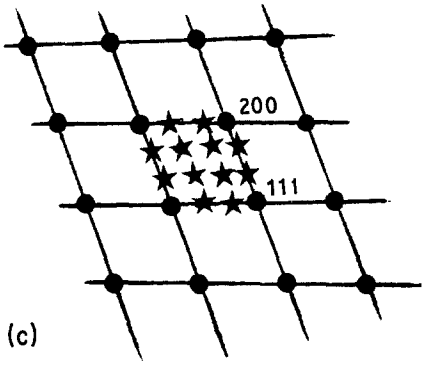

Figure 6 Ni–16.2 at.% B–1 at.% Ti alloy. (a) TEM observations of precipitation of the (τ) tau phase. (b) Diffraction pattern, and (c) key diagram: (●) Ni, (★) $Ni_{20}Ti_3B_6$.

and

$$\langle 0\,0\,1\rangle 1 \parallel \langle 0\,\bar{1}\,1\rangle 2$$

The boundary between the needles is straight, suggesting that there exists a strong crystallographic relationship between the two Ni_3B lattices. The orientation relationship between the two orientations of the Ni_3B needles seems to be the relationship obtained after a Bain transformation. This relationship is often observed in martensitic transformation in cubic systems [16]. The interface planes are (1 4 0)1 and (1 3 3)2, respectively, for the two kinds of Ni_3B needles.

In the intermediate region, a eutectoid-like structure is observed (Fig. 11c) between Ni_3B and Ni. The nickel lamellar spacing (50 to 100 nm) is always smaller than that of the Ni_3B ($\simeq$200 nm). In this region, the nickel lamellae increase in size until they

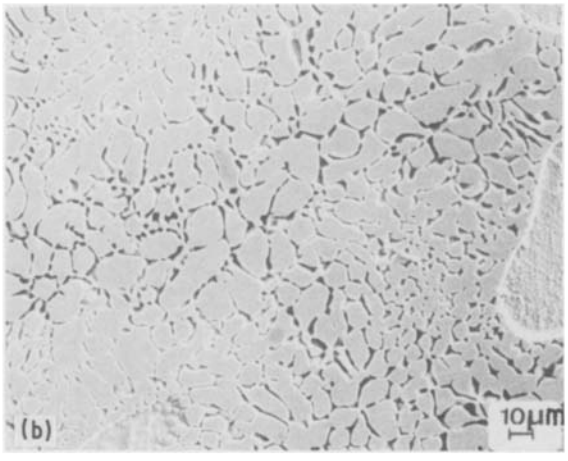

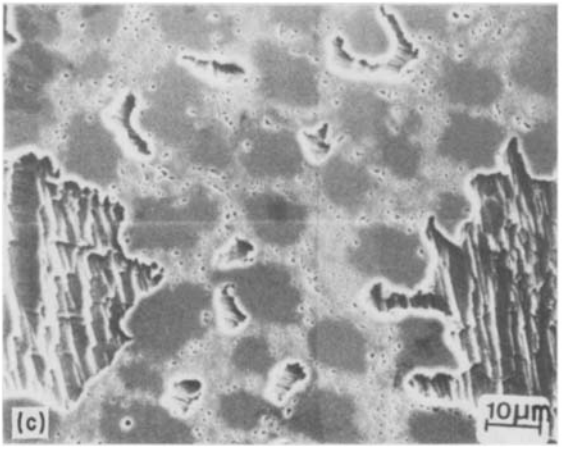

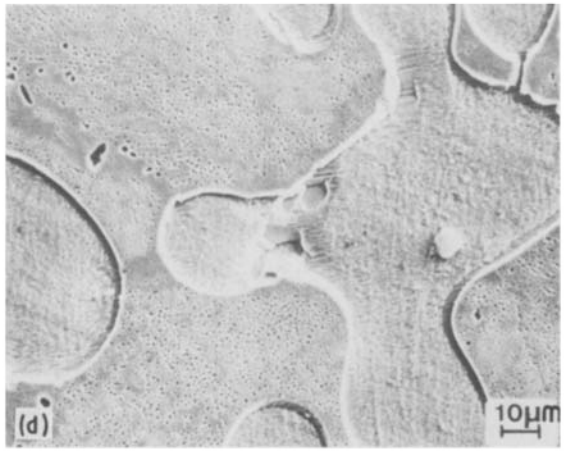

Figure 7 Microstructures of some slowly cooled doped (1 at.%) eutectic alloys (5° C min^{-1}). (a) Fe, (b) Al, (c) Ti, (d) V.

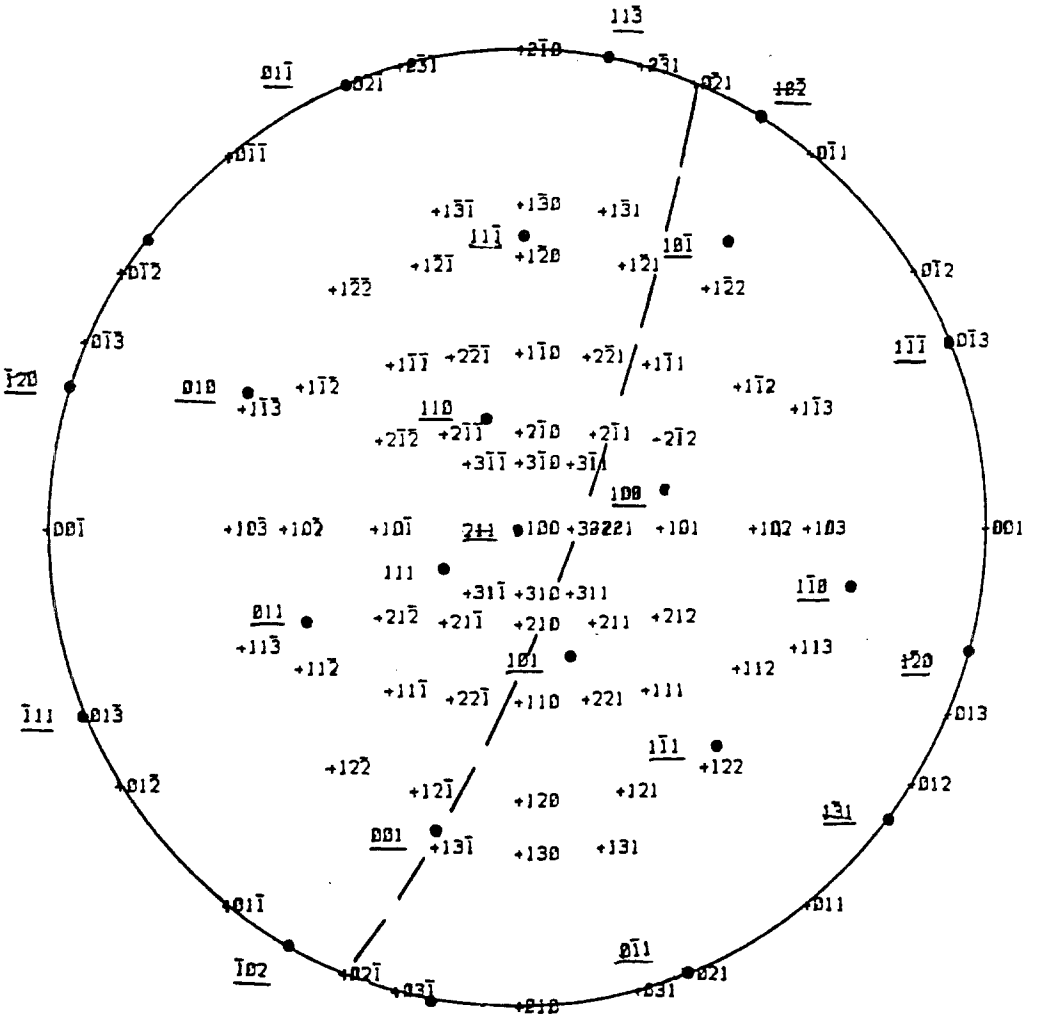

Figure 8 Superimposed stereogram for the orientation relationship of Ni–Ni_3B eutectic. (●) Ni, (+) Ni_3B.

reach almost 100 nm. We never observed larger nickel lamellae. The interface planes between Ni_3B and Ni in this region (II) remain parallel to the directions of the Ni_3B plates of region I. The orientation relationship between the two phases Ni_3B and Ni(α) in this region is completely different from those observed in the lamellar eutectic and seems to be directly related to the orientation of the Ni_3B needles.

In the internal region (III), we observed elongated nickel precipitates which are directly related to the crystallographic orientation of the Ni_3B matrix. These precipitates coarsen and become round. In this last region, we observed scattered almost spherical (from 100 to 200 nm) nickel precipitates. The largest are observed by SEM (Fig. 4b, c).

This particular structure is observed in binary systems in all the samples when cooled to room temperature and in ternary systems Ni–Ni_3B–(Cu, Ti, V). In the case of the slowly cooled Ti-doped eutectic alloy, deeper analysis on STEM–EDEX of the lamellar precipitates of nickel in the large Ni_3B phase show the presence of almost all the titanium in these nickel precipitates as shown in Fig. 13.

Moreover, this structure of Ni_3B may coexist in the same sample with the degenerate eutectic as shown in Fig. 14. In a quenched DTA sample at 810° C, the rough eutectic Ni–Ni_3B (Fig. 14a) is observed in the external part of the sample (Ni–16.2 at.% B). In the internal part, the complex structure of the Ni_3B is well in evidence (Fig. 14b).

The alloys which are slowly cooled (5° C min^{-1}) until room temperature show only this transformed phase in all the samples. Ageing followed by quenching in water at different temperatures gave rise to different structures. Our X-ray diffraction experiments on the alloys presenting these two different microstructures are well interpreted with the two phases Ni and Ni_3B, and did not show the existence of other compounds such as Ni_2B.

3.5. Comparison with some industrial alloys

Even in some commercial alloys, this complex structure of Ni_3B is observed. For comparison, two commercial brazing alloys (Alliages Frittes-Metafram SA) with low additional elements (wt %) have been examined. Alloy B (Ni–8% B–6% Si–7% Cr–1.2% Fe) is richer in additional elements than alloy A (Ni–6% B–4.8% Si–0.2% Fe). The microstructure of alloy B shows a solidification path (Fig. 15b) which is in agreement with the ternary liquidus projection Ni–B–Si [17]. Ni(α) dendrites are formed at 1170° C and are followed by the formation of two binary eutectics, Ni(α)–Ni_3B (975° C), then Ni_3B–Ni_5Si_2 (950° C). In DTA experiments, alloy A shows a transition at a low temperature (815° C). The microstructure of alloy A (less charged with additional elements) is comparable

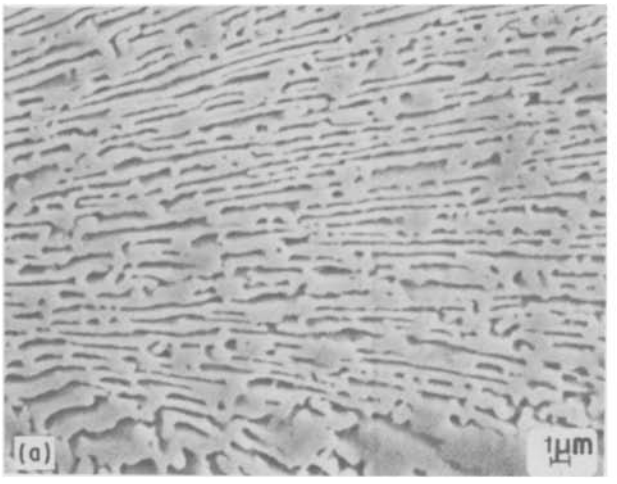

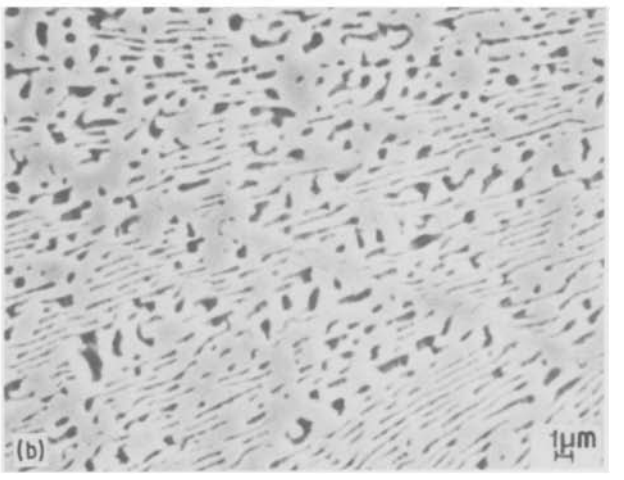

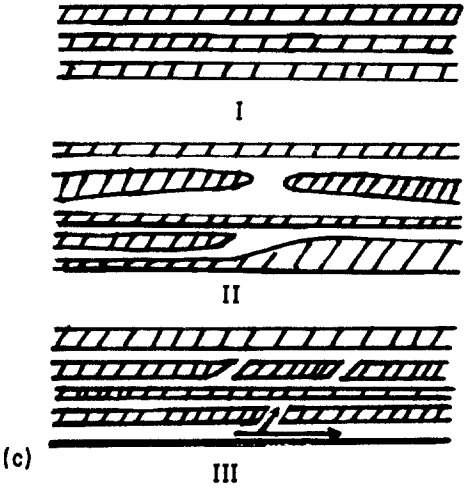

Figure 9 Coarsening of eutectic structure. (a) Aged 1 h at 900° C, (b) aged 2 h at 750° C then quenched, (c) schematic drawing of the changes in the interface between nickel and Ni_3B during coarsening.

to that of the slowly cooled binary Ni-rich Ni–B alloys (Fig. 15a). The Ni(α) dendrites (formed at 1270° C) contain some $\beta 1 Ni_3Si$ (L12) precipitates due to silicon segregation. The interdendritic phase is comparable to the transformed phase reported in Section 3.4.

4. Discussion

The discussion is divided into three parts. Firstly, we will try to explain the large undercooling observed in all these alloys during slow cooling in DTA experiments. Secondly, we will comment on the crystallography of the eutectic Ni–Ni_3B, the influence of the small amounts of additions and the rate of cooling. Lastly, we discuss the formation and the nature of the transformed structure observed in some of the alloys.

From our DTA results and microstructural observations in binary (Ni–B) and in ternary (Ni–B–M) systems, three typical morphologies are observed near the eutectic Ni–Ni_3B composition:

(i) a lamellar eutectic in quenched alloys and in the slowly cooled Fe-doped eutectic alloy. The formation of this lamellar eutectic is associated with a DTA exothermic peak between 1090 and 1110° C. But the

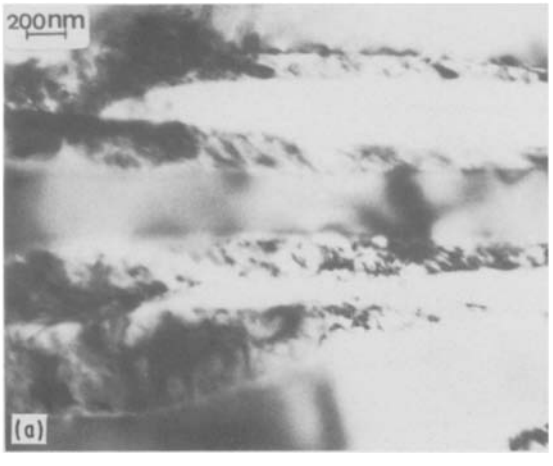

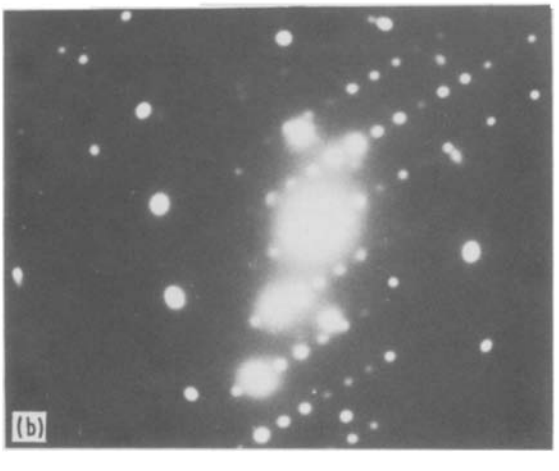

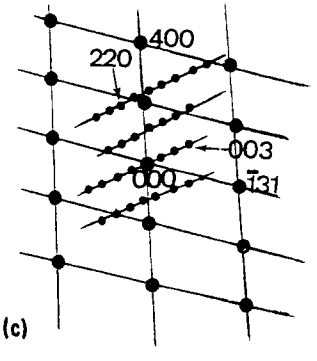

Figure 10 Ni–16.2 at.% B–1 at.% V alloy. (a) TEM observations of the lamellar eutectic between Ni(α) and Ni_3B. (b) Diffraction pattern, and (c) key diagram: (●) Ni, (•) Ni_3B.

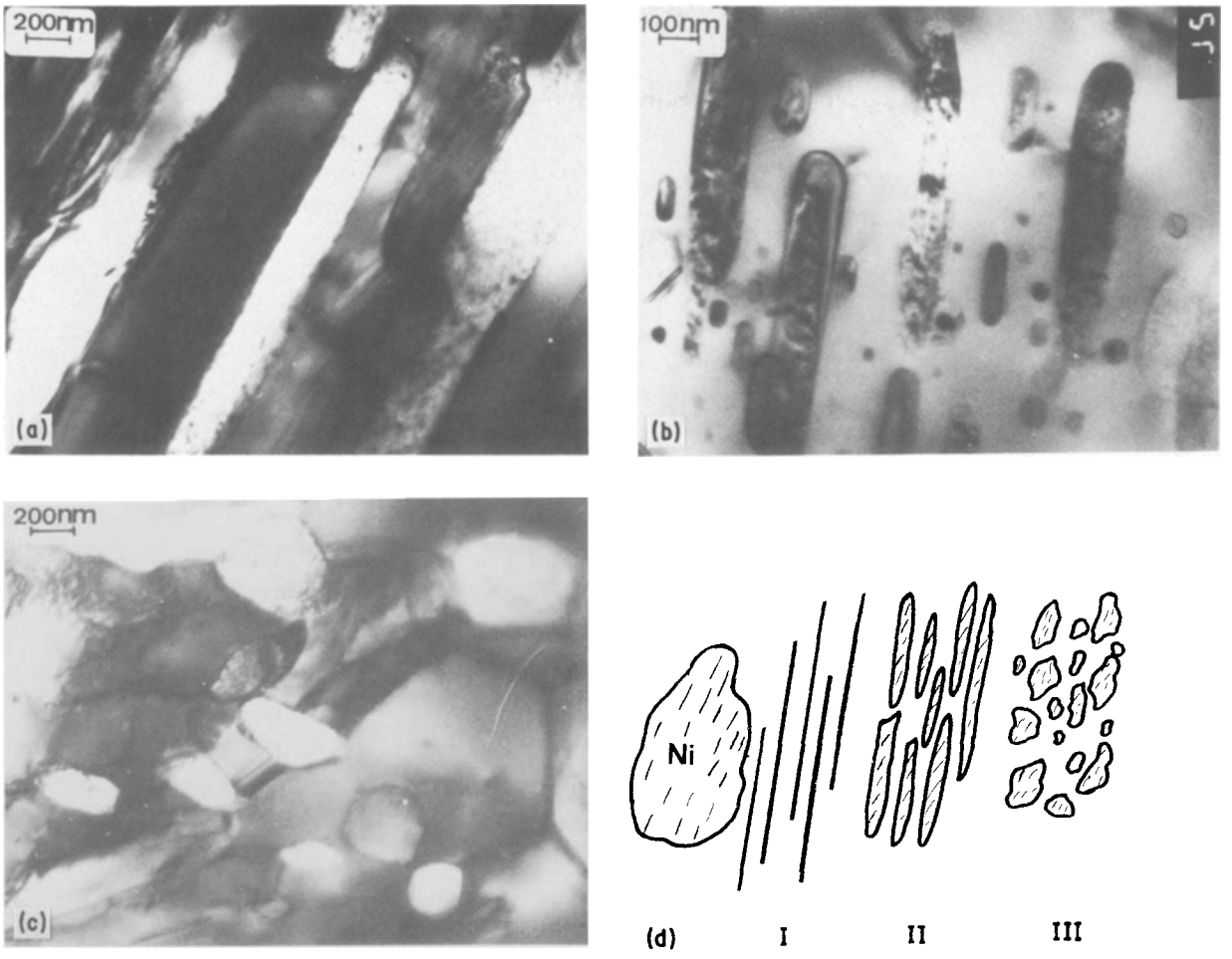

Figure 11 Different features of Ni_3B observed in the slowly cooled Ni–19.2 at.% B alloy.

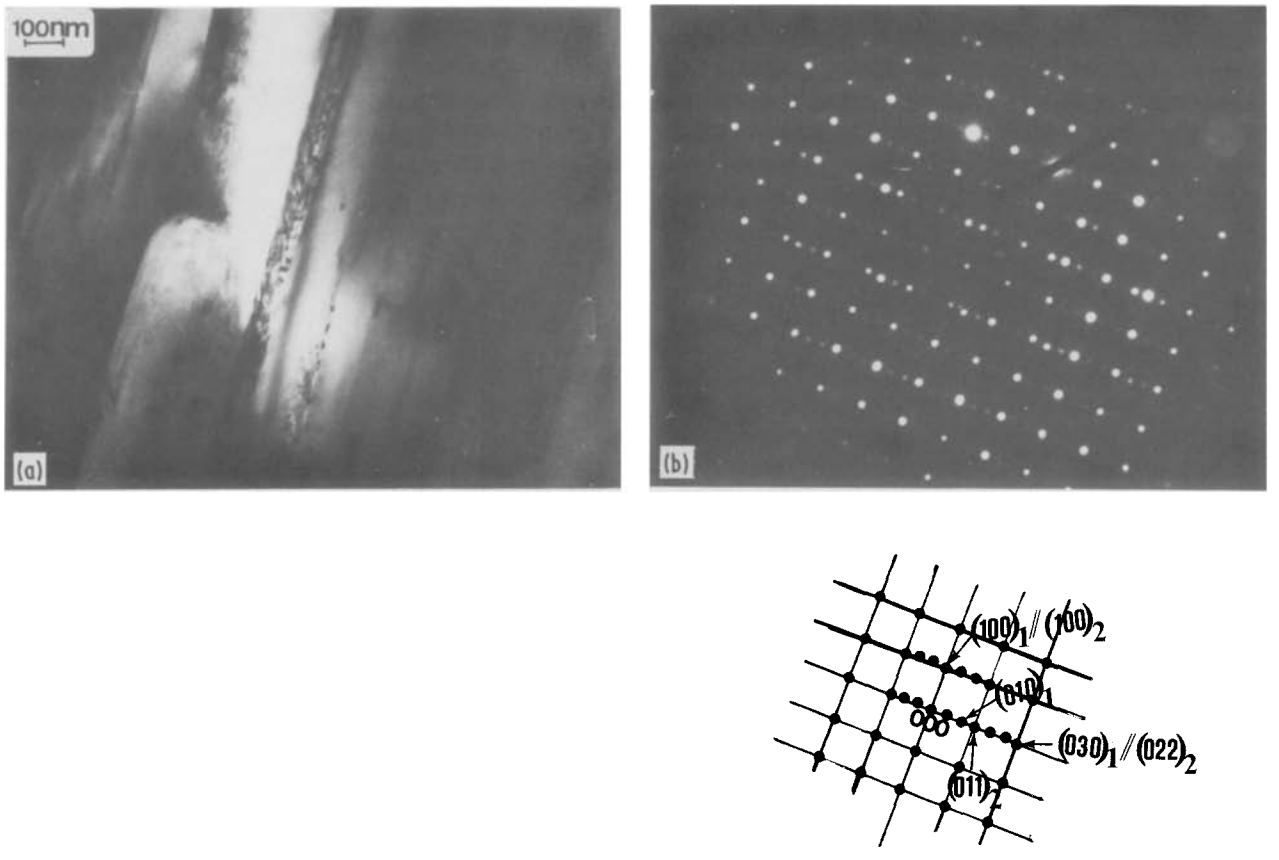

Figure 12 Crystallographic orientation relationship between two laths of Ni_3B in the Ni–19.2 at. % B alloy.

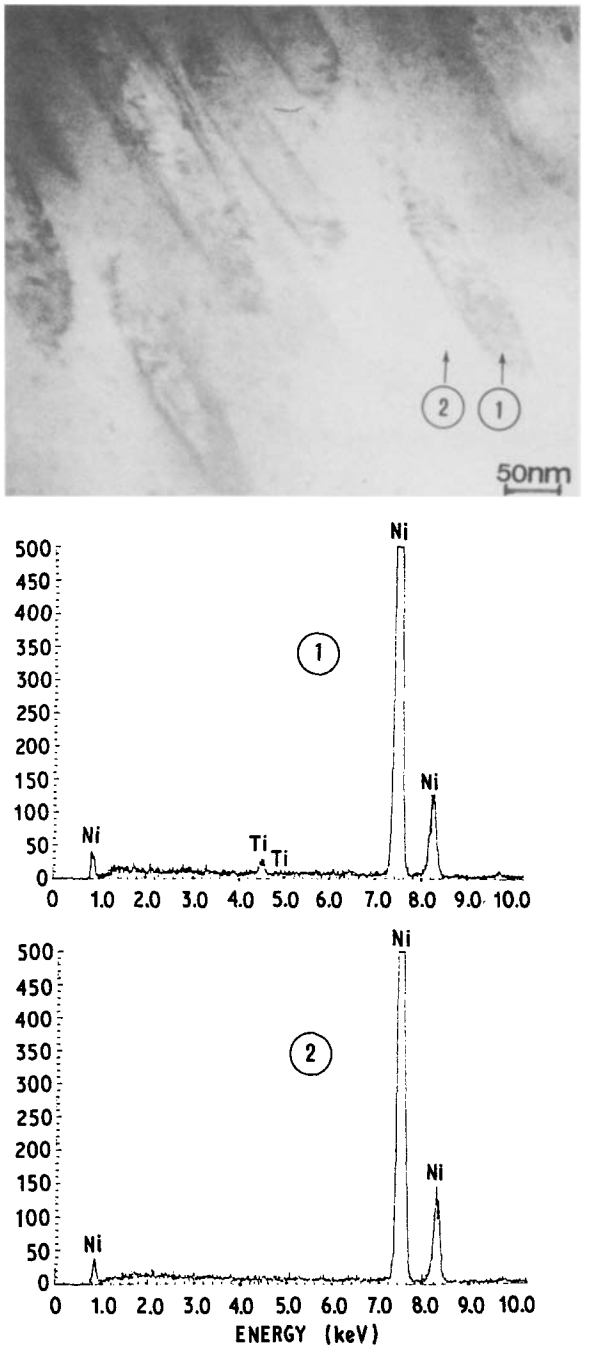

Figure 13 STEM observations of the Ni_3B phase in the slowly cooled Ti-doped binary eutectic alloy.

orientation relationship between Ni(α) and Ni_3B is different in the two cases;

(ii) a degenerate eutectic which is observed either in the binary Ni–B system without or with some additions (chromium, aluminium). In this microstructure, Ni(α) dendrites are observed at a larger extent than expected on the phase diagram. Even hypereutectic alloys (20 at.% B) show small amounts of Ni(α) dendrites. The formation of this degenerate eutectic consisting of large islands of Ni_3B is associated, during cooling, with a DTA exothermic peak near 970° C;

(iii) a large Ni_3B phase with some internal precipitates. This structure is observed in all the binary alloys (< 30 at.% B) slowly cooled until room temperature and in some ternary alloys Ni–Ni_3B–(Cu, Ti, V). As in the last case, a large number of Ni(α) dendrites are observed. This interdendritic structure appears as made up of large Ni_3B phase with laths of Ni_3B well oriented and some Ni(α) precipitates. This structure is associated with the exothermic peak at low temperature between 950 and 800° C.

These last two morphologies may coexist in the same sample (Fig. 14) depending on the locality in the centre or on the border of the DTA ingot. Moreover, in some cases, the three morphologies have been observed within the same sample.

4.1. Solidification behaviour

The beginning of the solidification of the primary phase in some of the slowly cooled doped eutectic alloys is higher than the temperature of the same transition in the binary eutectic alloys without or with iron and chromium additions. The addition of aluminium, titanium, copper or vanadium effectively increases the temperature of the beginning of solidification of the primary phases Ni(α) near 1145° C.

In agreement with previous authors, we observed that all alloys with low boron content (< 30 at.%) in the Ni_3B region show large undercooling. The behaviour during heating and cooling in DTA experiments is very different. The melting temperature of the eutectic Ni–Ni_3B (1110° C) is in good agreement with all other results: 1110° C for Portnoi *et al.* [8], 1093° C

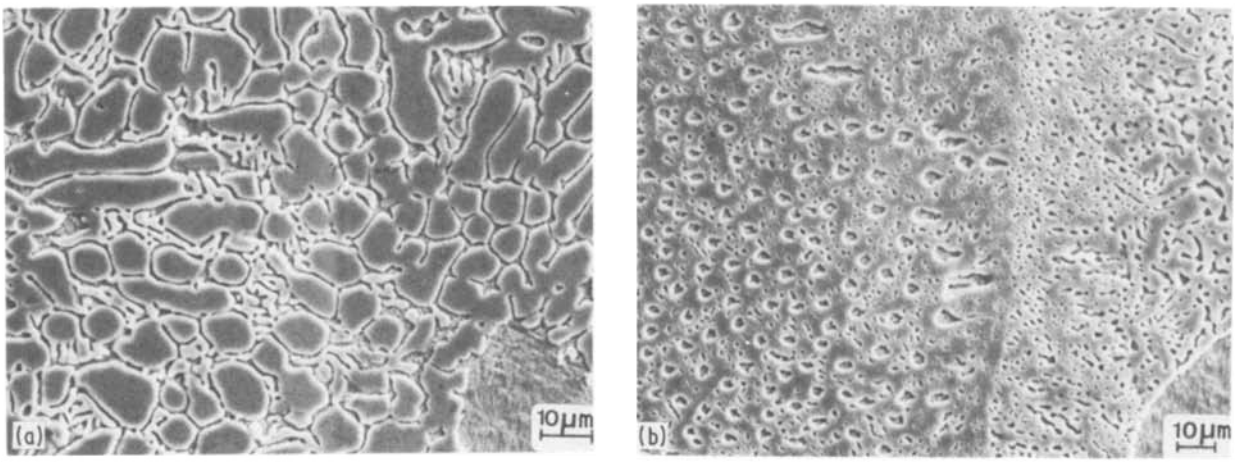

Figure 14 Structure of DTA sample (Ni–16.2 at.% B) quenched from 810° C showing eutectic structure between Ni_3B and Ni in (a) the external part and (b) in the centre of the ingot.

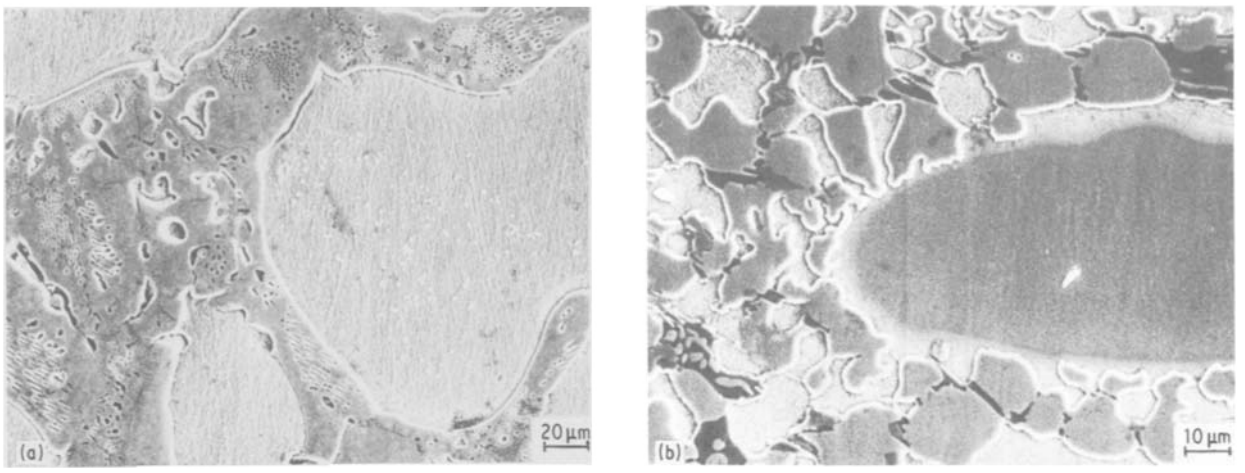

Figure 15 Microstructure of two commercial alloys showing different features of Ni–Ni_3B eutectic.

for Schöbel and Stadelmaier [9] and 1045° C for Sobolev and Fedorov [11].

Schöbel and Stadelmaier [9], studying the binary system Ni–B, interpreted the large undercooling observed in low boron content alloys as due to the formation of a metastable eutectic between Ni(α) and Ni_2B at 986° C. They mentioned that they never observed Ni_2B and interpreted these results by a solid state transformation of the metastable Ni_2B phase at a temperature below 900° C into the stable phase Ni_3B. We also never observed Ni_2B either in X-ray diffraction or in electron diffraction. Sobolev and Fedorov [11] explained the undercooling by the difficulty of formation of the compound Ni_3B from the melt.

During slow cooling, the hypo- or hyper-eutectic alloys (B < 20 at.%) all start to solidify with Ni(α) which nucleates more easily than Ni_3B in the liquid. The Ni(α) grows until it reaches the point where the undercooling necessary for the nucleation of Ni_3B in the presence of nickel is sufficient. At this point, the liquid is supersaturated with elemental boron and the nucleation of Ni_3B phase is possible in all the liquids [18, 19]. With a cooling rate of 5° C min^{-1}, the total undercooling, ΔT, required for the nucleation of Ni_3B phase in the presence of Ni(α) is 240° C determined in the same manner as by several other authors [20, 21].

Even in the rapidly cooled alloys, the nucleation of Ni_3B seems to be difficult in the presence of Ni(α). From our results on the quenched Ni–B alloys, a large halo of Ni_3B is formed during cooling around the Ni(α) dendrites as shown in Figs 2a and 5a. The liquid around the Ni(α) primary phase moves along the metastable line, past the eutectic point and becomes supersaturated with the Ni_3B phase. Before the eutectic can freeze, the excess of the Ni_3B has to freeze as a halo around the Ni(α) dendrites. This halo of Ni_3B nucleates the Ni(α) phase and the lamellar eutectic Ni(α)–Ni_3B grows as seen in Fig. 5a. When the cooling is rapid, the temperature of the liquid drops below the line of nucleation of nickel where the nickel is nucleated by Ni_3B and the eutectic lamellar is grown.

In the presence of aluminium or chromium additions, the nucleation of Ni_3B requires a large undercooling. The nucleation occurs at the point (980° C–20 at.% B). The nucleation of Ni_3B phase occurs in all the melt and the eutectic appears as a globular degenerate eutectic with some of the remaining Ni(α) between the islands of Ni_3B. If M = silicon, copper or vanadium or without additions, nucleation of Ni_3B takes place with a higher undercooling than with aluminium or chromium additions (970, 950° C,–22 at.% B). The amount of Ni(α) primary dendrites is larger than expected and the remaining Ni(α) is too low to surround the globular Ni_3B and this phase appears as the large transformed phase. The DTA exothermic peak between 1000 and 950° C is associated with the nucleation of Ni_3B.

4.2. Coupled solidification and crystallography of the lamellar eutectic Ni(α)–Ni_3B

The second part of this discussion concerns the structure of the lamellar eutectic observed during cooling. The nickel boride Ni_3B has an orthorhombic structure (Pbnm) as reported in Table I [7, 22], and is isomorphous with Fe_3C and $NiAl_3$.

The crystallography of the unidirectionally solidified eutectic Ni–Ni_3B was previously investigated by Shapiro and Ford [12]. These authors proposed an orientation relationship between Ni(α) and Ni_3B described as

$$(1\,0\,3)Ni_3B \parallel (0\,0\,1)Ni$$

and

$$\langle 3\,1\,1\rangle Ni_3B \parallel \langle 1\,1\,0\rangle Ni$$

In the slowly-cooled Fe-doped eutectic alloys, the orientation relationship between the two phases as observed in Section 3.3 is well represented by the relation given by Shapiro and Ford. However, the two orientation relationships, ours (in the case of rapidly cooled alloys) and those of Shapiro and Ford [12], are deduced from each other by a rotation of 30° of the (1 1 1)Ni plane around the (1 0 0)Ni_3B plane. The (1 0 0)Ni_3B plane is almost parallel to the (2 1 1)Ni plane. The (1 1 1)Ni plane is parallel to the (0 1 3) and the (0 1 1) Ni_3B planes, respectively, in our experiments and in Shapiro and Ford's results. Based on the

TABLE IV Summary of lattice misfit between Ni and Ni_3B

Ni lattice spacing		Ni_3B lattice spacing		$\Delta a/a$
hkl	*d*(*hkl*)	*hkl*	*d*(*hkl*)	
111	2.032	013	2.026	0.003
002	1.76	103	1.968	0.12
022	1.245	042	1.210	0.03
111*	2.032	022*	2.042	0.008
002*	1.76	113*	1.84	0.05

*Lattice misfit from Shapiro and Ford [12].

mutual relationships of the two crystals, Table IV summarizes the amount of lattice misfit for some planes. In the two cases, the small degrees of misfit (0.5 to 5%) indicate a good fitting between low reticular planes.

The structure of Ni_3B is of Fe_3C type. The eutectic Ni–Ni_3B is, therefore, analogous to that between austenite and cementite. Furthermore, the Ni–B system is not susceptible to the reaction austenite f c c $\rightleftharpoons$ c c as in Fe–C alloys. Inoue and Matsumoto [23] observed rapidly solidified high carbon Cr–W and Cr–Mo steels. The microstructure of as quenched ($10^{6\circ}$ C sec^{-1}) of a (3.6C–3.4W–18.6Cr) steel shows a lamellar structure consisting of austenite matrix and cementite Fe_3C. The high cooling rate could be enough to suppress the precipitation of usual carbides M_7C_3 and $M_{23}C_6$ and the transformations from austenite to ferrite as ordinarily observed. From selected-area diffraction patterns, these authors observed an orientation relationship between γ-Fe and Fe_3C which is in good agreement with our observations in the isostructural rapidly cooled Ni–Ni_3B eutectic.

Many studies have been devoted to the coarsening of lamellar or rod-like eutectics. We observed that the coarsening was initiated at faults, as did Graham and Kraft [15] in their studies of Al–Al_2Cu eutectic. As the Ni_3B recedes from faults and thickens during heat treatment, it seems that the controlling process involves diffusion through the Ni(α) phase rather than diffusion through the Ni_3B phase. The diffusing species (certainly boron) is difficult to determine because the diffusion coefficient of boron in nickel is not known. From Graham and Kraft, the diffusion of aluminium in aluminium of the Al–Al_2Cu controls the thickening of the eutectic. However, in Al–Al_3Ni (which is isostructural with Ni_3B), the coarsening is controlled by the diffusion of nickel in the aluminium phase [24].

However, all these authors [15, 24] never observed changes in the crystallographic relationship or interface plane during the thickening process of the lamellar specimens. During ageing of binary lamellar eutectic Ni–Ni_3B, we observed a reorientation of the crystallographic structure in the coarsening regions. After ageing at 900° C for 1 h, the plane of the interface is at about 70° with respect to the original uncoarsened lamellae. It seems that the discrepancy observed between our results in the rapidly cooled eutectics, and the results of Shapiro and Ford, or those obtained in the slowly cooled Fe-doped eutectic alloys may be explained by energetic considerations. In the rapidly cooled samples, the orientation relationship is metastable and is governed by the formation of a low energetic interface. The relationship obtained in the slowly cooled alloys is the stable one and can be obtained either during slow cooling or reorganization of the rapidly cooled eutectic.

4.3. Precipitation and solid state transformation of Ni_3B during slow cooling

As reported in Section 3.4, the solidification behaviour during cooling of most of these alloys is complicated. Considering the alloy compositions in the neighbourhood of point N (Fig. 1), after the formation of the primary phase Ni(α), associated with the first transition during cooling in DTA experiments, the remaining liquid composition becomes extremely saturated with boron atoms and the solidification of a Ni_3B phase very rich in nickel occurs. This transition is associated with the second transition observed in DTA at about 970° C. This Ni_3B phase, supersaturated with nickel atoms, is associated with the needle-like structure shown in Fig. 11a. As the temperature decreases the Ni_3B(Ni) saturated with nickel atoms transforms into an eutectoid-like lamellar structure by rejecting the excess nickel atoms to the interface of the needles, thus forming the Ni_3B with stoichiometric composition and the rejected Ni(α), i.e.

$$Ni_3B(Ni) \rightarrow Ni_3B + Ni(\alpha)$$

$$\Delta H = 4.8\,cal\,g^{-1}\,(20\,kJ\,kg^{-1})$$

This transformation is associated with the third and last exothermic peak between 950 and 800° C in DTA. This eutectoid-like structure resulting from the above reaction is shown in Fig. 11b, d (II). This same argument applies for the slowly cooled binary eutectic alloys with additional elements such as titanium, which present the same transformed structure (Fig. 13). In this case, the non-stoichiometric Ni_3B is saturated with the atoms of nickel and titanium at the same time. The rejection of these atoms of nickel and titanium to the interface gives rise to the same eutectoid-like lamellar structure observed in Fig. 13

$$Ni_3B(Ni, Ti) \rightarrow Ni_3B + Ni(Ti)$$

This explains why all the titanium is found in the nickel lamellae as shown in Fig. 13.

Moreover, the lamellar eutectoid-like structure and the quantity of heat released associated with this transformation can be compared with that associated with the eutectoid reaction usually observed in the Fe–C system

$$\gamma(Fe) \rightarrow \alpha(Fe) + Fe3C$$

$$\Delta H = 4.3\,cal\,g^{-1}\,(18.1\,kJ\,kg^{-1}).$$

After the formation of this lamellar eutectoid-like structure, it becomes more or less spherical as the temperature decreases due to coarsening in order to obtain the most stable form. Furthermore, as shown in Fig. 15, this type of transformation is also observed in industrial alloys during slow cooling.

To the best of our knowledge, this type of transformation has never been reported before in the Ni–B

alloys. Recently, Pliz and Ryder [25], in amorphous $Ni_{78}B_{14}Si_8$ alloys, show that after heat treatment for 1 h at 430° C, precipitates having a fine lamellar structure nucleate on the primary Ni(α) crystals. These authors are unable to decide whether the precipitates consist of Ni_3B or a eutectoid of this phase with nickel.

5. Conclusion

This work shows the importance of small amounts of additions (often neglected) in experimental considerations and the effects they can have on the interpretation of results. The influence of the cooling rate on these alloys is very important, as shown by the different types of structures obtained with respect to the cooling rates.

A solid state transformation of Ni_3B of eutectoid-like type is also observed during cooling in binary Ni–B eutectic alloys or in binary alloys with additions such as titanium, vanadium or silicon.

References

1. O. KNOTEK and E. LUGSCHEIDER, *J. Vac. Sci. Technol.* **11** (1974) 798.
2. E. A. ANTONOVA, N. S. ANDRUSHENKO and L. M. SINAI, *Zatshita Metallov* 7 (1971) 137.
3. H. T. STEINE and W. SIMM, *Int. J. Powder Metall. Powder Technol.* **18** (1982) 57.
4. S. LEBAILI and S. HAMAR-THIBAULT, *Mem. Sci. Rev. Met.* (1984) 519.
5. P. T. KOLOMYTSEV, *Izv. An. SSSR, Otd. Khim. N. Met. i Toplivo* **3** (1960) 83.
6. L. H. ANDERSON and R. KIESSLING, *Acta Chem. Scand.* **4** (1933) 160.
7. S. RUNDQVIST, *ibid.* **12** (1958) 658.
8. K. I. PORTNOI, V. M. ROMASOV, V. M. CHUBAROV, M. Kh. LEVINSKAYA and S. E. SALIBEKOV, *Poroshkovaya Metallurgiya* **50** (1967) 15.
9. A. S. SCHOBEL and H. H. STADELMAIER, *Z. Metallkde* **56** (1965) 856.
10. B. O. JANSSON and J. AGREN, *Mater. Sci. Engng* **63** (1984) 51.
11. A. S. SOBOLEV and T. F. FEDOROV, *Izvestiya Akad. Nauk SSSR, Neorg. Mater.* **4** (1967) 723.
12. S. SHAPIRO and J. A. FORD, *Trans. Met. Soc. AIME* **233** (1965) 334.
13. I. COUMES, R. HAMAR and S. HAMAR-THIBAULT, *J. Thermal Anal.* **32** (1987) 425.
14. A. S. SCHOBEL and H. H. STADELMAIER, *Metall.* **19** (1965) 715.
15. L. D. GRAHAM and R. W. KRAFT, *Trans. Met. Soc. AIME* **236** (1966) 94.
16. C. WAYNMAN, "Physical Metallurgy", edited by . Cahn (Elsevier, 1983) Ch. 15.
17. S. LEBAILI and S. HAMAR-THIBAULT, *Acta Metall.* **35** (1987) 701.
18. L. F. MONDOLFO, *J. Aust. Inst. Met.* **10** (1965) 169.
19. S. E. SUNDQUIST, R. BRUSCATO and L. F. MONDOLFO, *J. Inst. Met.* **91** (1962) 204.
20. B. CANTOR and R. D. DOHERTY, *Acta Metall.* **33** (1979) 33.
21. R. H. SOUTHIN and G. A. CHADWICK, *ibid.* **26** (1978) 223.
22. C. B. FINCH, O. B. CAVIN and P. F. BECHER, *J. Cryst. Growth* **67** (1984) 556.
23. A. INOUE and T. MATSUMOTO, *Met. Trans.* **11A** (1980) 739.
24. H. B. SMARTT and T. H. CORTNEY, *ibid.* **7A** (1976) 123.
25. O. PILZ and P. L. RYDER, 5th International Conference on Quenched Metals, Würzburg, Germany (1984), edited by . Steeb, H. Warlimont, (North Holland, 1985) p. 377.
26. H. J. GOLDSMITH, "Interstitial Alloys" London, (Butterworths, 1965).

Received 12 June
and accepted 27 August 1987